Chain Persistence Length and Structure in Hyaluronan Solutions: Ionic Strength Dependence for a Model Semirigid Polyelectrolyte

Eric Buhler*,† and François Boué‡

Groupe de Dynamique des Phases Condensées, UMR No. 5581, CC 26, Université de Montpellier II, 34095 Montpellier Cedex 5, Centre de Recherches sur les Macromolécules Végétales-CNRS, UPR No. 5301, Joseph Fourier University, BP 53, 38041 Grenoble Cedex 9, and Laboratoire Léon Brillouin (CEA-CNRS), CEA Saclay, 91191 Gif/Yvette, France

Received October 6, 2002; Revised Manuscript Received November 4, 2003

ABSTRACT: In this study, we have directly determined for the first time the structure and the chain conformation of hyaluronan, a model semirigid polyelectrolyte polysaccharide. At high ionic strength, detailed information on the chain flexibility has been obtained from combined light and small-angle neutron scattering experiments by applying different fitting methods based upon expressions for a single-chain scattering function of a wormlike chain without excluded volume. Particular attention has been given to the determination of the intrinsic persistence length, L_0, and a value close to 90 Å was found using the different fitting procedures. Without screening (i.e., at low ionic strength), the measured total persistence length appears increased by at least the amount predicted by Odijk for the electrostatic contribution, L_e ($\sim\kappa^{-2}$, square of the Debye−Hückel screening length). This would mean this model was checked using classical polyelectrolytes. At high ionic strength the scattered intensity crosses over, with decreasing q, from a q^{-1} rod to a q^{-2} coil variation as predicted for a wormlike chain. Conversely, at low ionic strength it crosses over from a q^{-1} to a q^{-4} (or q^{-3}) variation, characteristic of polymer associations. These associations are also observed in our dynamic light scattering measurements, with a behavior very similar to that of flexible polyelectrolytes.

1. Introduction

We report here small-angle neutron scattering (SANS), static light scattering (SLS), and dynamic light scattering (DLS) first measurements of the structure and chain conformation of a bacterial polysaccharide, hyaluronan (HA). Hyaluronan belongs to a class of water-soluble polysaccharides, bearing charges in water, which can be called semirigid polyelectrolytes. This means that, apart from electrostatic effects, the chain backbone is locally stiff enough to correspond to an intrinsic persistence length L_0 much larger than the monomer length. L_0 can be measured when the electrostatic repulsions are screened by addition of salt. Very few physical studies were performed on semirigid polyelectrolyte solutions.[1,2]

When electrostatic repulsions between the charges along the semirigid chain in aqueous solutions are not screened, they will tend to make even larger the local rigidity and increase the global size of the polyion. The commonly used mean field models for polyelectrolytes usually divide the total persistence length, L_T, into an electrostatic persistence length, L_e (due to electrostatic repulsions between neighbor ionic sites), and the intrinsic persistence length, L_0, such that[3]

$$L_T = L_0 + L_e \tag{1}$$

The total persistence length L_T accounts for the effective rigidity of the polyelectrolyte through the sum of two contributions: the intrinsic persistence length L_0 of the corresponding uncharged chain and the electrostatic persistence length L_e. L_e will depend on electrostatic screening in the solution, i.e., on ionic strength, which is due to counterions as well as external salt concentration. For semirigid polyelectrolyte polysaccharides, L_0 is easily larger than L_e (at least for external salt concentration larger than 3×10^{-3} M). For such a case ($L_e \ll L_0$, or at least $L_e < L_0$), several theoretical models[3−6] that report calculations of L_e have been presented in the past. A frequently used model to calculate L_e is the so-called OSF theory, which has independently been derived by Odijk,[3] Skolnick, and Fixman.[4] Assuming a Debye−Hückel potential and under the condition that cation condensation occurs when necessary,[7] they found

$$L_e = \frac{\zeta^2}{4\kappa^2 l_B} \quad \text{for} \quad \zeta < 1 \quad \text{(OSF relation)} \tag{2}$$

where $l_B = e^2/\epsilon_0 kT = 7.13$ Å in water is the Bjerrum length (ϵ_0 is the dielectric permittivity of the solvent and e the elementary charge) and κ^{-1} is the Debye−Hückel screening length related to the concentration of the counterions. For hyaluronan, the distance between two ionic sites, equal to the monomer length $a = 10.2$ Å, is larger than l_B; in other words the structural charge parameter ζ is lower than 1: $\zeta = l_B/a = 0.7$. Manning's counterion condensation expected when $a < l_B$ ($\zeta > 1$), bringing the distance between charges equal to l_B, is not of relevance here. In dilute polyelectrolyte solutions

$$\kappa^2 = 4\pi l_B c_f \tag{3}$$

In eq 3, c_f is the concentration of free monovalent ions. Since $\zeta < 1$, $c_f = c + 2c_s$, where c is the monomer concentration and c_s the excess salt concentration. OSF eq 2 is valid if $\kappa L_T \gg 1$, which is true for polyelectrolyte near the rod limit or at least for polyelectrolytes having a high L_0. In this model L_e is proposed to be proportional

† Université de Montpellier II and Joseph Fourier University.
‡ CEA Saclay.

10.1021/ma0215520 CCC: $27.50
Published on Web 01/17/2004

Table 1. Variation of the Intrinsic Viscosity, Overlap Concentration, Second Virial Coefficient, Radius of Gyration, Diffusion Coefficient, Hydrodynamic Radius, and Dynamical Second Virial Coefficient as a Function of the Hyaluronan Molecular Weight in 0.1 M NaCl Solutions

M_w	$[\eta]$ (cm^3/g)	c^* (g/cm^3)	$10^4 A_2$ [($cm^3 \cdot mol)/g^2$]	R_G (Å)	$10^{-7} D_0$ (nm^2/s)	R_H (Å)	k_D (cm^3/g)
85×10^3	330 ± 50	3×10^{-3}	9.5 ± 1.0	270 ± 20	2.1 ± 0.2	116 ± 10	44 ± 5
160×10^3	500 ± 50	2×10^{-3}	8 ± 1	350 ± 40	1.23 ± 0.12	170 ± 20	38 ± 5

to c_f^{-1}. A series of papers[8−10] demonstrate that aqueous solutions of giant polymer-like nonionic micelles (i.e., wormlike micelles) "doped" with small amounts of ionic surfactants serve as ideal model systems for "equilibrium semirigid polyelectrolytes". These authors have made a quantitative comparison among OSF theory, Monte Carlo computer simulations, and small-angle neutron scattering and light scattering experiments. In these studies, both Monte Carlo and scattering experimental data seem to converge to OSF theory. However, this variation was never checked experimentally with classical polyelectrolytes to our knowledge. From the experimental point of view, one must find the best classical semirigid polyelectrolyte for testing eq 2. Also, if L_0 is much smaller, variational calculations have shown that the flexibility of the backbone rules out the OSF reasoning.[11] L_T measurements obtained till now in such a flexible case with classical polyelectrolytes (polystyrene sulfonate sodium), after subtraction of L_0 from L_T (i.e., applying relation 1), lead to a variation of L_e closer[12−14] to $c_s^{-1/2}$. However, one must note that recent and complete computer simulations have predicted a variation of L_e with κ^{-2} for long flexible polyelectrolytes (with 4096 charged monomers) composed of electrostatic blobs.[15,16] On the other hand, for rigid polyelectrolytes (such as DNA with $L_0 \approx 500$ Å), eq 2 should apply, but the electrostatic contribution does not increase strongly the rigidity of the chain ($L_e \ll L_0$). The intermediate semirigid case of hyaluronan proposed here may be revealed as interesting since (i) L_0 is not too large (∼86 Å), (ii) L_T can be measured by SANS in the available q range, (iii) L_e is more than a small perturbation, (iv) the dependence of L_e on the ionic strength can be checked in good conditions (if no polyelectrolyte associations appear in low ionic strength solutions), and (v) hyaluronan is a classical semirigid polyelectrolyte.

In this paper, we will try to access the chain conformation in the dilute regime, which will be possible at high ionic strength, under strong screening. This will give us the total persistence length in conditions where the electrostatic contribution is naught. Then we will investigate the ionic strength dependence of the chain persistence length for low screening. We will see that some information on the total persistence length (and therefore on the electrostatic contribution) is accessible, but that some associations between chains are also visible at lower scattering wave vectors. Also, dynamical measurements show that the association behavior at low ionic strength is similar for flexible and semiflexible polyelectrolytes. In this paper is described the full and complete experimental investigation of the structural and dynamical properties of hyaluronan solutions. A previous paper, reporting SANS results and where Figures 2a, 7, and 10 are presented, was already published.[17]

2. Materials and Methods

2.1. Sample Characteristics. We have investigated aqueous solutions of the polysaccharide polyelectrolyte hyaluronan of molecular weight equal to 85×10^3 and 160×10^3 (determined using light scattering measurements). Hyaluronan is a linear semirigid polysaccharide (helical structure), with the repeating disaccharide structure poly[(1→3)-β-D-GlcNAc-(1→4)-β-D-GlcA]. Bacteria synthesize it, but different varieties are also found in animals and humans. We used bacterial hyaluronan produced and carefully purified under the Na salt form by Soliance (Pomacle, France). The structure of hyaluronan was checked using NMR experiments. The molecular weight $M_w = 85\,000$ was obtained by acid hydrolysis and determined by GPC and light scattering. The polydispersity (determined using GPC experiments) is equal to the ratio $M_w/M_n = 1.3$, where M_w is the weight-average molecular weight and M_n the number-average molecular weight. The mass of a monomer unit is equal to $m = 400$ g/mol, the length of a monomer is equal to $a = 10.2$ Å, and the weight-averaged contour length is equal to $L_c = 2170$ and 4080 Å for the 85 K and 160 K samples, respectively. The aqueous solutions were investigated in the polymer concentration range from $c = 2.5 \times 10^{-4}$ g/cm^3 to $c = 1.5 \times 10^{-2}$ g/cm^3 in the dilute and semidilute regimes at the temperature $T = 25$ °C. The excess salt concentration, i.e., the NaCl concentration, varies from 0 to 0.1 M. The solutions were filtered through 0.2 μm Sartorius cellulose nitrate membranes. The light scattering measurements were performed on the same solutions as used for the small-angle neutron scattering experiments (i.e., aqueous solutions of D_2O) and within the same week. Moreover, SLS measurements were carried out before and after the SANS experiments to check whether no degradations occur with the natural polymer hyaluronan, and no changes were observed with time.

Dilute and semidilute regimes are separated by the critical overlap concentration c^*, i.e., when $c[\eta]$ is about unity.[18] $[\eta]$ is the intrinsic viscosity of the solution and η the solution viscosity. Values of $[\eta]$ and c^* for the different studied 0.1 M NaCl hyaluronan solutions (M_w = 85 K and 160 K) are collected in Table 1.

2.2. Viscosity Measurements. The viscosity measurements were carried out by using a low-shear 40 coaxial viscometer, on the Newtonian plateau, within the range of polymer concentration from 2×10^{-4} to 2×10^{-3} g/cm^3 (dilute regime).

2.3. Static Light Scattering. SLS and DLS experiments were performed by means of a spectrometer equipped with an argon ion laser (Spectra Physics model 2020) operating at λ = 488 nm, an ALV-5000 correlator (ALV, Langen-Germany Instruments), a computer-controlled and stepping-motor-driven variable-angle detection system, and a temperature-controlled sample cell. The temperature was 25 ± 0.1 °C unless otherwise noted. The scattering spectrum was measured through a band-pass filter (488 nm) and a pinhole (200 μm for the static experiments and 100 or 50 μm for the dynamic experiments) with a photomultiplier tube (ALV).

In the SLS experiments, the excess of scattered intensity $I(q)$ was measured with respect to the solvent, where the magnitude of the scattering wave vector q is given by

$$q = \frac{4\pi n}{\lambda} \sin \frac{\theta}{2} \tag{4}$$

In eq 4, n is the refractive index of the solvent (1.34 for water at 25 °C), λ is the wavelength of light in the vacuum, and θ is the scattering angle. In our experiments, the scattering angle θ was varied between 20° and 150°, which corresponds to scattering wave vectors q in the range from 5.95×10^{-4} to 3.31×10^{-3} Å^{-1}. The absolute scattering intensities $I(q)$ (i.e.,

the excess Rayleigh ratio) were deduced using a toluene sample reference for which the Rayleigh ratio is well-known, i.e., 40 $\times 10^{-6}$ cm^{-1} at 488 nm.[19]

The virial expression for the osmotic pressure can be used in the dilute regime to deduce the following relationship:

$$\frac{Kc}{I(q,c)} = \frac{1}{M_w}\left[1 + q^2\frac{R_G^2}{3} + ...\right] + 2A_2Q(q,c)c + ... \quad (5)$$

The function $Q(q,c)$ is approximately unity for flexible polymer chains, but not for spheres;[19] $Q(0,c)$ is equal to 1 in any case. c is the polymer concentration, and A_2 is the second virial coefficient, which describes the polymer−solvent interactions. The scattering constant is $K = 4\pi^2n^2(dn/dc)^2/N_A\lambda^4$, where dn/dc is the refractive index increment and N_A is Avogadro's number. The dn/dc of the polysaccharide hyaluronan in the solvent 0.1 M NaCl/water is equal to 0.140.[1] The plots of $c/I(q,c)$ versus q^2 were extrapolated to $q = 0$ to give intercepts $c/I(0,c)$. If the probed length scale q^{-1} is sufficiently large compared to the radius of gyration R_G of the polymers, the form factor obeys Guinier's law and the apparent radius of gyration $R_{G,app}$ can be determined from the intercept and the initial slope of these plots using a scattering inverse Lorentzian law of the form[19]

$$\frac{c}{I(q,c)} = \frac{c}{I(0,c)}\left[1 + \frac{q^2R_{G,app}^2}{3}\right] \quad \text{if} \quad qR_G \ll 1 \quad (6)$$

The weight-average molecular weight[19] M_w can be obtained from

$$\frac{I(0,c)}{Kc} = M_{w,app} = M_w(1 - 2A_2M_wc) \quad (7)$$

The apparent weight $M_{w,app}$ of polymers in solution at a concentration c is given by extrapolation of the scattered intensity $I(q)/c$ to $q = 0$, while the apparent radius of gyration is obtained by a mean-square linear fit of the inverse of the scattered intensity versus q^2.

2.4. Dynamic Light Scattering. In the DLS experiments, the normalized time autocorrelation function $g^{(2)}(q,t)$ of the scattered intensity is measured:[19]

$$g^{(2)}(q,t) = \frac{\langle I(q,0)\, I(q,t)\rangle}{\langle I(q,0)\rangle^2} \quad (8)$$

The latter can be expressed in terms of the field autocorrelation function or equivalently in terms of the autocorrelation function of the concentration fluctuations $g^{(1)}(q,t)$ through

$$g^{(2)}(q,t) = A + \beta|g^{(1)}(q,t)|^2 \quad (9)$$

where A is the baseline and β is the coherence factor, which in our experiments is equal to 0.7−0.9. The normalized dynamical correlation function $g^{(1)}(q,t)$ of polymer concentration fluctuations is defined as

$$g^{(1)}(q,t) = \frac{\langle \delta c(q,0)\, \delta c(q,t)\rangle}{\langle \delta c(q,0)^2\rangle} \quad (10)$$

where $\delta c(q,t)$ and $\delta c(q,0)$ represent fluctuations of polymer concentration at time t and zero, respectively.

In our experiments, the inspection of the angular dependence shows that the relaxations are diffusive with all characteristic times inversely proportioned to q^2. Some of our solutions were characterized by a single relaxation mechanism. For these solutions we have adopted the classical cumulant analysis.[20] This analysis provides the variance of the correlation function and the first reduced cumulant $(\tau q^2)^{-1}$, where τ is the average relaxation time of $g^{(1)}(q,t)$. The extrapolation of $(\tau q^2)^{-1}$ to $q = 0$ yields the values of the mutual diffusion constant D. The latter is related to the average hydrodynamic radius R_H of the macromolecules through

$$D = \frac{kT}{6\pi\eta_sR_H} = \left(\frac{1}{\tau q^2}\right)_{q^2=0} \quad (11)$$

where k is the Boltzmann constant, η_s the solvent viscosity, and T the absolute temperature.

Some other solutions showed several relaxation mechanisms (low ionic strength solutions); then we used a more appropriate method to determine the average relaxation time τ: the Contin method based on the inverse Laplace transform of $g^{(1)}(q,t)$.[21] If the spectral profile of the scattered light can be described by a multi-Lorentzian curve, then $g^{(1)}(q,t)$ can be written as

$$g^{(1)}(q,t) = \int_0^\infty G(\Gamma)\exp(-\Gamma t)\, d\Gamma \quad (12)$$

where $G(\Gamma)$ is the normalized decay constant distribution.

2.5. Small-Angle Neutron Scattering. SANS experiments were carried out on the spectrometer PACE in the Léon Brillouin Laboratory at Saclay (Orphée reactor, France). The chosen incident wavelength λ depends on the set of experiments, as given below. For a given wavelength, the range of the amplitude of the transfer wave vector q was selected by changing the detector distance D. We report here measurements for one unique polymer concentration ($c = 1.5 \times 10^{-3}$ g/cm^3) and several ionic strengths. In the first experiment ([NaCl] = 0.1 M, high ionic strength solution; see Figures 1 and 2), we used three settings: in the first we explore a q range of $3 \times 10^{-3} \le q$ (Å^{-1}) $\le 3.3 \times 10^{-2}$ (distance to detector D = 4.65 m, wavelength $\lambda = 13.14 \pm 1.00$ Å), in the second a q range of $5 \times 10^{-3} \le q$ (Å^{-1}) $\le 5.33 \times 10^{-2}$ (D = 4.65 m, $\lambda = 8.09 \pm 0.50$ Å), and in the third a q range of $1.37 \times 10^{-2} \le q$ (Å^{-1}) $\le 1.45 \times 10^{-1}$ (D = 2.264 m, $\lambda = 6.06 \pm 0.50$ Å). In the second and third experiments ([NaCl] = 6×10^{-3} and 10^{-3} M, low ionic strength solutions; see Figures 6 and 7), we used two settings: $3.17 \times 10^{-3} \le q$ (Å^{-1}) $\le 3.37 \times 10^{-2}$ (D = 4.65 m, $\lambda = 13.17 \pm 1.00$ Å) and $6.1 \times 10^{-3} \le q$ (Å^{-1}) $\le 6.48 \times 10^{-2}$ (D = 3.09 m, $\lambda = 10 \pm 1$ Å). At last, in the fourth experiment ([NaCl] = 0 M, low ionic strength solution; see Figure 8), we used two settings: $3.27 \times 10^{-3} \le q$ (Å^{-1}) $\le 3.48 \times 10^{-2}$ (D = 4.52 m, $\lambda = 13.18 \pm 1.00$ Å) and $6.2 \times 10^{-3} \le q$ (Å^{-1}) $\le 6.54 \times 10^{-2}$ (D = 3.193 m, $\lambda = 9.88 \pm 1.00$ Å).

The data are put on an absolute scale following the standard procedures. Intensities relative to the incoherent scattering of H_2O in a cell with a path of 1 mm are obtained from the measured intensities after subtraction of the solvent and empty cell contributions. The electronic and neutronic background was subtracted for the measurements at low q; it is negligible for the high-q configurations. Using direct beam measurements, the final spectra can be given in absolute units of cross section (cm^{-1}). The running time for one sample (i.e., one solution and one solvent background of given ionic strength) is around 4 days because the level of the scattered intensity of the dilute hyaluronan solutions is very low. To obtain a very good statistic with our data, the solvent background measurements were obtained using the same long running time as used for the solution.

It is possible to combine data from light and neutron static scattering covering these different but overlapping q ranges. Both the neutron and the light scattering data have been normalized to give absolute scale units in cm^{-1}. Therefore, it is still necessary to rescale the SLS data to give the overlap with the SANS data. This scaling factor is equal to the ratio between the SANS contrast and the SLS contrast, i.e., ∼2300. The light scattering intensity at each q value was adjusted by this constant factor so that the SLS data overlap with the SANS data in the region of comparable q. The scattering profiles cover then a q range of nearly 3 decades.

3. Results and Discussion

We will describe successively the data for the two situations of screening: first high ionic strength solutions and then low ionic strength solutions.

3.1. High Ionic Strength Solutions. This part deals with light and neutron scattering experiments performed on 0.1 M NaCl aqueous solutions of 85 K hyaluronan. SANS experiments were only performed in the dilute regime, at a unique polymer concentration $c = 1.5 \times 10^{-3}$ g/cm^3 for 85 K hyaluronan solutions.

3.1.1. Static Light Scattering in the Dilute Regime: Guinier Regime $qR_G \ll 1$. Static light scattering experiments performed under 0.1 M NaCl hyaluronan dilute solutions allowed us to appreciate the degree of interaction between the chains, via the second virial coefficient A_2. For the 85 K hyaluronan sample, we indeed confirmed a behavior corresponding to the dilute regime, since the solution structure factor follows $S^{-1}(q = 0) \approx 1 + 2A_2M_wc$, with $A_2 = (9.5 \pm 1.0) \times 10^{-4}$ (cm^3·mol)/g^2, a rather small value. Therefore, we can assume the solutions studied in this part to be dilute. For such dilute 85 K hyaluronan solutions, the radius of gyration $\langle R_G\rangle_0 = 270$ Å was determined from the SLS experiments using eq 5 in the regime $qR_G \ll 1$. For 160 K hyaluronan, A_2 is similarly small (8×10^{-4} (cm^3·mol)/g^2), and $\langle R_G\rangle_0 = 350$ Å. Error bars together with values of R_G and A_2 are collected in Table 1.

Benoît and Doty[22] have calculated the radius of gyration $\langle R_G^2\rangle_0$ of a wormlike chain in Θ conditions using the persistence length L_0 and the contour length L_c:

$$\langle R_G^2\rangle_0 = \frac{(L_cL_0)}{3} - L_0^2 + \frac{2L_0^3}{L_c} - \frac{2L_0^4}{L_c^2}\left[1 - \exp\left(\frac{-L_c}{L_0}\right)\right] \quad (13)$$

This "wormlike" chain model serves as a bridge between the rod limit, where $L_0 \gg L_c$ and $\langle R_G^2\rangle_0 = L_c^2/12$, and the random coil limit, where $L_c \gg L_0$ and $\langle R_G^2\rangle_0 = L_cL_0/3$. Equation 13 applies only to semirigid molecules in which there are no excluded volume effects. We can assume this is the case since A_2 is small. In the case of strong screening considered in this section, the electrostatic repulsions are screened ($L_e \approx 1.5$ Å ≈ 0 and $\kappa^{-1} \approx 10$ Å, according to eq 2); thus, the total persistence length is approximately equal to the intrinsic one. Hence, the behavior of the hyaluronan chain should be close to that of a Gaussian chain. This makes it possible to deduce from the value of the radius of gyration the intrinsic persistence length using the Benoît and Doty relation given above for $L_0/L_c \ll 1$: $L_0 = 3R_G^2/L_c = 218700/2170 = 100 \pm 15$ Å. For 160 K hyaluronan, the same reasoning yields $L_0 = 90 \pm 20$ Å.

Now we determine the polydispersity effect on our data. Using eq 13 and assuming a Schulz−Zimm-type distribution for the chain length, Schmidt[23] has calculated an analytical expression for the radius of gyration for polydisperse wormlike chains:

$$\langle R_G^2\rangle_0 = \frac{m+2}{3y}L_0 - L_0^2 + \frac{2y}{m+1}L_0^3 - \frac{2}{m(m+1)}L_0^4\left(y^2 - \frac{y^{m+2}}{(y + L_0^{-1})^m}\right) \quad (14)$$

where $y = (m + 1)/L_c$ and $m = 1/(M_w/M_n - 1)$, L_c being in this case the weight-average contour length of the polymer and $M_w/M_n = 1.3$. The limiting behavior for a Gaussian coil, where $\langle R_G^2\rangle_0 = [(m + 2)/(m + 1)](L_cL_0/3)$, and for a rigid rod, where $\langle R_G^2\rangle_0 = [(m + 3)(m + 2)/(m + 1)^2](L_c^2/12)$, are recovered for $L_c \gg L_0$ and $L_c \ll L_0$, respectively. This also makes it possible to deduce the intrinsic persistence length L_0 of the hyaluronan Gaussian polydisperse chains, $L_0 = 82 \pm 15$ Å for the 85 K sample, and the same reasoning yields $L_0 = 73 \pm 20$ Å for the 160 K sample. One can say that, if we compare with the experimental values obtained in the previous paragraph, neglecting polydispersity will lead to a small overestimation of L_0 in our case. In the literature authors have shown[23] that neglecting polydispersity will lead to an overestimation of L_0. However, most of their studies (e.g., xanthan) were realized under much more polydisperse samples ($M_w/M_n \approx 2$).

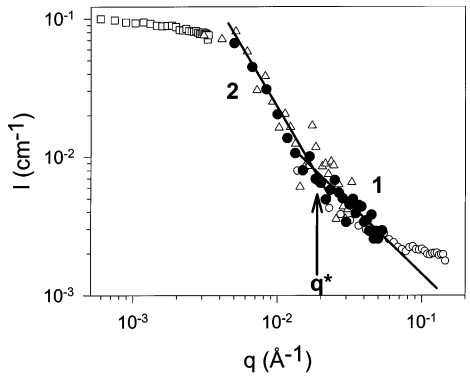

Figure 1. Variation of the scattered intensity, I, with q over four q ranges: $5.95 \times 10^{-4} \le q$ (Å^{-1}) $\le 3.31 \times 10^{-3}$ (SLS, □); $3 \times 10^{-3} \le q$ (Å^{-1}) $\le 3.3 \times 10^{-2}$ (△); $5 \times 10^{-3} \le q$ (Å^{-1}) $\le 5.33 \times 10^{-2}$ (●); $1.37 \times 10^{-2} \le q$ (Å^{-1}) $\le 1.45 \times 10^{-1}$ (○). Black lines with slopes respectively equal to 2 and 1 are guides for the eye. The NaCl concentration is equal to 0.1 M (high ionic strength) and the polymer concentration to 1.5×10^{-3} g/cm^3.

3.1.2. Small-Angle Neutron Scattering and the Intermediate Regime: $qR_G \gg 1$. We now investigate the intermediate q range of the scattered intensity to achieve a quantitative evaluation of the persistence length, L_T, or Kuhn length, L_k, where $L_k = 2L_T$. The usual equation for absolute neutron scattering by macromolecules in solution combines the form factor $P(q)$ of the polymer with the interparticle scattering factor[19] $S_2(q)$. The factor $S_2(q)$ reflects the interactions between the segments of two different chains ("pair term"). In the following equation, we have separated the "self" and "pair" particle contributions to the total intensity:[19]

$$I(q)\ (\mathrm{cm}^{-1}) = \frac{1}{V}\frac{\mathrm{d}\sigma}{\mathrm{d}\Omega} = (\Delta\rho)^2(\phi_{vol}V_{chain}P(q) + S_2(q)) \quad (15)$$

$(\Delta\rho)^2 = (\rho_{HA} - \rho_{D_2O})^2$ is the contrast factor per unit volume between the polymer and the solvent and was determined from the known chemical composition. $\rho = \sum n_ib_i/(\sum m_iv/N_A)$ represents the scattering length per unit volume, b_i is the neutron scattering length of the species i, m_i the mass of species i, and v the specific volume of hyaluronan (0.59 cm^3/g) or D_2O. $V_{chain} = Nvm/N_A$ is the volume of the N monomers (of mass $m = 400$ g/mol each) in a chain and $\phi_{vol} = cv$ is the volume fraction of monomer, N_A being Avogadro's number. In dilute and high ionic strength polymer solutions, where intermolecular effects should be diminished, we will assume that the scattering is arising from isolated chains without interactions and without excluded volume; i.e., $S_2(q) \approx 0$, and thus, $I(q) \propto P(q)$.

First we look at neutron scattering data, i.e., mostly at the intermediate regime ($qR_G \gg 1$). As shown in Figure 1 (log−log plot), representing the variation of the

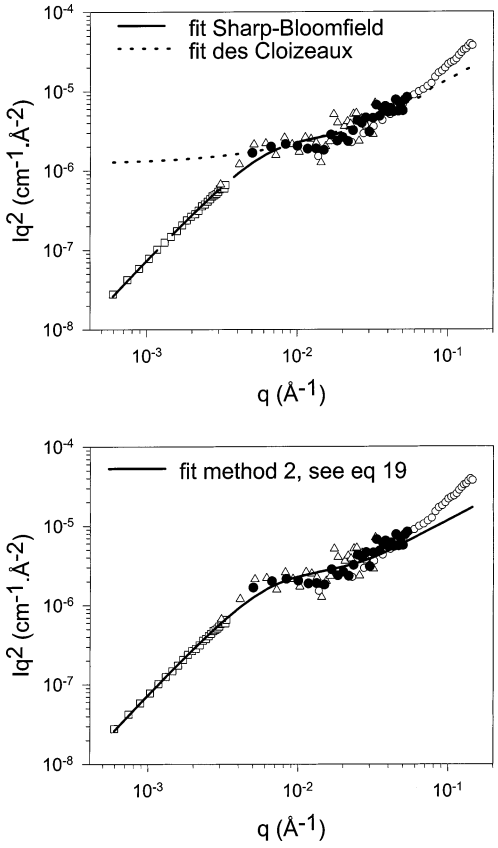

Figure 2. (a) Kratky plot, variation of Iq^2 with q over four q ranges: $5.95 \times 10^{-4} \leq q$ (Å^{-1}) $\leq 3.31 \times 10^{-3}$ (SLS, □); $3 \times 10^{-3} \leq q$ (Å^{-1}) $\leq 3.3 \times 10^{-2}$ (△); $5 \times 10^{-3} \leq q$ (Å^{-1}) $\leq 5.33 \times 10^{-2}$ (●); $1.37 \times 10^{-2} \leq q$ (Å^{-1}) $\leq 1.45 \times 10^{-1}$ (○). Reprinted with permission from ref 17. Copyright 2003 Springer. The dashed lines represent the fits of the data obtained with the des Cloizeaux (---; $qL_T > 2$) and Sharp−Bloomfield (− − −; $qL_T < 2$) expressions (see method 1). The NaCl concentration is equal to 0.1 M (high ionic strength) and the polymer concentration to 1.5×10^{-3} g/cm^3. (b) Variation of Iq^2 with q. The solid line represents the fit of the data obtained using method 2, i.e., using a single expression for $P(q)$ valid over the entire q range (see eq 19).

scattered intensity with q over the four investigated q ranges (SLS and SANS) for a $c = 1.5 \times 10^{-3}$ g/cm^3 dilute 85 K hyaluronan solution, the scattering in this regime displays a crossover between two regimes. The first asymptotic regime corresponds to polymer coils and the form factor decays with a power law of the form $P(q) \approx q^{-2}$. At larger values of q, $P(q)$ is controlled by smaller distances than L_T over which polymers are rodlike, and we observe a crossover to an asymptotic q^{-1} dependence for $P(q)$, which is typical for locally rod structures. In such a case, one usually represents scattering data by a "Kratky plot" [24a] of the product $I(q)q^2$ as a function of q as is shown in Figure 2 over the four investigated q ranges (SLS and SANS). The Kratky plot is ideally suited to visualize the distinct scaling regions discussed in context with Figure 2, and it directly demonstrates the crossover from a rigid rodlike to a coillike behavior at the length scale of L_T. Note that a Holtzer plot (Iq versus q) is also ideally suited to visualize the distinct scaling regions.[24b] For shorter chains with no well-developed coil plateau, it makes sense to choose a bending rod plot (Holtzer) rather than a Kratky one.[24b] In our case, the coil plateau is sufficiently extended and the Kratky representation is convincing. Actually, in the high-q-range domain ($q > 0.08$ Å^{-1}) we observe a departure from the q^{-1} rod behavior. But one must note that the scattering length scale q^{-1} is on the same order in this regime as the length of a monomer unit (10.2 Å). We see then details of the monomer shape inside the solvent (well-described by Rawiso many years ago[24a]), which are beyond our scope.

3.1.3. Methods for Fitting the Whole Scattering: Determination of the Flexibility. Due to the very low scattering of the dilute solutions, the SANS experiments were performed at the unique polymer concentration $c = 1.5 \times 10^{-3}$ g/cm^3. First of all, we have assumed that the residual excluded volume effect obtained from the estimate of $S(q=0)$ based on the second virial expansion using the value of A_2 is negligible at high q, i.e., in the q range where the persistence length L_T is determined. Also the influence of excluded volume effects as well as the incorporation of interchain interactions in the intermediate q range is usually not included in the interpretation of small-angle scattering data. However, note that Jerke et al.[25] have shown that interaction effects will not only influence the apparent molar mass obtained at $q = 0$, but also the values of the apparent persistence length due to the influence of $S(q)$ at intermediate q values, even at relatively low concentrations $c < c^*$. Results from a many-chain Monte Carlo simulation of the wormlike chain model have indeed demonstrated that interaction effects do influence the structure factor even in the q region used to determine L_T. To estimate the true persistence length, we thus should have made an extrapolation to $c = 0$. However, in the present case, at slightly higher q than the Guinier regime, the scattered intensity crosses over to a power law behavior with an exponent equal to −2, characteristic of a chain in the Θ regime (which is wide for a short chain such as ours) and not of a chain in good solvent conditions for which the exponent is about −5/3. Moreover, apart from electrostatic excluded volume, water is not necessarily a good solvent for a polysaccharide such as hyaluronan. Finally, (i) according to ref 26, excluded volume effects are only important for chains with $M_W > 10^6$ [26] (which is not our case), and (ii) $L_e \approx 0$ and $\kappa^{-1} \approx 10$ Å (screened conditions according to eq 2). We have then used expressions derived for chains without excluded volume to fit the whole scattering. In this context we have used two different methods to determine L_T.

(i) Method 1. In the first method we have fitted the q^2I curve over the four q ranges (see Figure 2a) to the Sharp−Bloomfield[27] form factor $P_{SB}(q)$ of a single finite wormlike chain of contour length L_c:

$$P_{SB}(q) = \frac{2[\exp(-x) + x - 1]}{x^2} + \left[\frac{4}{15} + \frac{7}{15x} - \left(\frac{11}{15} + \frac{7}{15x}\right)\exp(-x)\right]\frac{2L_T}{L_c} \quad (16)$$

with $x = L_cL_Tq^2/3$. Equation 16 is a valid approximation only for $L_c > 10L_T$ in a q range of $qL_T < 2$. For $qL_T = 2$, the values overlap[28] the exact calculation of des Cloizeaux[29] for chains of infinite length. The des Cloizeaux expression will then be used for $qL_T > 2$:

$$P_{Cloizeaux}(q) = \frac{\pi}{qL_c} + \frac{2}{3q^2L_TL_c} \quad (17)$$

The Kratky plot provides a sensitive way to test the agreement between theoretical and experimental scattered intensity. Data in the q range $q > 0.08$ Å^{-1} (details of the monomer) were not used for the fit. The L_T value is obtained by fitting the data in the whole experimental q range with simultaneously the Sharp−Bloomfield equation ($qL_T < 2$) and the des Cloizeaux equation ($qL_T > 2$). Finally, the two parameters characterizing the fit of the data $L_0 \approx L_T = 86.5$ Å and $L_c = 2311$ Å are obtained. The fit is not very sensitive to the slight connection problem between SLS and SANS data. It allows a smooth adjustment, which reinforces the quality of our fit. This is also checked with the obtained value of L_0 in very good agreement with the direct determination given above from R_G if we use Benoît and Doty's relation. Also, the L_c value is very close from the estimated theoretical value $Na = 2170$ Å, with $N = 85\,000/400$.

About the use of the Sharp−Bloomfield expression, we note that, from a comparison of Monte Carlo simulations and model calculations, Pedersen and Schurtenberger[26] pointed out that this is only satisfactory for small qL_T, i.e., for $qL_T < 1$ instead of $qL_T < 2$. Actually, in the present case, the results of the fit using the Sharp and Bloomfield expression in a q range of $qL_T < 1$ are pretty close to the results obtained in a q range of $qL_T < 2$. However, these authors[26] have derived a more appropriate and recent model fitting approach and have calculated a single expression for $P(q)$ that is valid over the entire range of q values. The results obtained using this fitting procedure are presented in the following paragraph and in Figure 2b (method 2).

(ii) Method 2. Part of the method derived by Pedersen and Schurtenberger[26] is based on the expressions used by Burchard and Kajiwara[30] for chains without excluded volume effects in which the scattering form factor calculated by Sharp and Bloomfield[27] is used at low q. They used a crossover to the asymptotic scattering of a rod at high q by means of a simple empirical crossover function. The scattering Sharp−Bloomfield function, $P_{SB}(q)$ (see eq 16), agrees with the correct function for $qL_T < 1$. Also, at high q, Burchard and Kajiwara[30] suggested to approximate the scattering function by

$$P_{loc}(q) = \frac{1}{2L_cL_Tq^2} + \frac{\pi}{L_cq} \tag{18}$$

where the subscript indicates that the equation should reproduce the local rodlike structure. To fit our experimental data over the entire q range, we used the following single interpolation expression:

$$P(q) = P_{SB}(q)\exp\left[-\left(\frac{2qL_T}{\alpha}\right)^{\beta}\right] + P_{loc}(q)\left(1 - \exp\left[-\left(\frac{2qL_T}{\alpha}\right)^{\beta}\right]\right) \tag{19}$$

where α and β are empirical constants. Pedersen and Schurtenberger have shown that this expression can be used for $L_c > 4L_T$, and have optimized the values of the parameters α and β by a least-squares fit of eq 19 to the simulated scattering functions assuming a 1% error on the data. We then used[26] $\alpha = 5.53$ and $\beta = 5.33$. Due to the rather large polydispersity index of hyaluronan ($M_w/M_n = 1.3$), the contour length was a fitting parameter. The fit of the data is presented in Figure 2b, and the two parameters characterizing the fit are obtained: $L_T \approx L_0 = 90.3$ Å and $L_c = 2031$ Å, values in very good agreement with the results obtained using method 1.

3.1.4. Dynamic Light Scattering. The general picture for dilute semiflexible polyelectrolyte solutions, in the presence of an excess of salt ([NaCl] = 0.1 M) that screens the electrostatic interactions, is that the dynamical structure factor $g^{(1)}(q,t)$ is found to be characterized by a simple monoexponential diffusive relaxation; i.e., the characteristic relaxation time is q^{-2}-dependent. Also, it is observed that the apparent diffusion coefficient D measured is a linear function of the polyelectrolyte concentration:

$$D = D_0(1 + k_Dc + ...) \tag{20}$$

with D_0 the apparent diffusion coefficient at infinite dilution and k_D the dynamical second virial coefficient. Using the Stockes−Einstein equation (see eq 11), we can calculate the hydrodynamic radius R_H using the value of D_0. Such a picture applies for our [NaCl] = 0.1 M solution. The small positive value of k_D (44 cm^3/g) found here for the 85 K hyaluronan solution indicates and confirms that the electrostatic interactions are screened. The hydrodynamic radius of the polymer chains is related to D_0 through eq 11. Values of D_0, R_H, and k_D for the two studied hyaluronan molecular weight samples are collected in Table 1.

The separation between the dilute and semidilute regimes is characterized by the critical overlap concentration. We have estimated it, above in the text, as $c^* = 3 \times 10^{-3}$ g/cm^3 for the 0.1 M NaCl 85 K hyaluronan solution; i.e., $c^*[\eta]$ is about unity.[18] $[\eta] = 330$ cm^3/g is the intrinsic viscosity of the 85 K hyaluronan solution and η the viscosity of the solution ([NaCl] = 0.1 M). In the semidilute regime, the apparent diffusion coefficient D increases consequently with polymer concentration. In this regime, the variation of the fast diffusion coefficient can be described by a power law: $D \approx c^{0.90}$. de Gennes developed a scaling theory for semidilute solutions of neutral chains in thermodynamically good solvents.[18] The main prediction of this theory is that the dynamical behavior of the solution can be described in terms of a single characteristic length, that is, the correlation length ξ. Then the cooperative diffusion coefficient is given by

$$D = \frac{kT}{6\pi\eta_s\xi_H} \tag{21}$$

where ξ_H is the hydrodynamic correlation length that scales like the static correlation length ξ. The correlation length and consequently the cooperative diffusion coefficient D follow simple scaling laws of dilution according to[18]

$$\xi \approx c^{-0.77} \quad \text{and} \quad D \approx c^{0.77} \tag{22}$$

The concentration dependence of the apparent hydrodynamic radius in the dilute regime and of the correlation length in the semidilute regime is presented in Figure 3. The crossover value between constancy and decrease (showed by an arrow in Figure 3) occurs at a concentration value close to our estimate of c^*. In the semidilute regime, the concentration dependence of the correlation length is rather close to those of flexible neutral polymers. A value larger than 0.77 can be explained by the fact that the behavior of the chains is

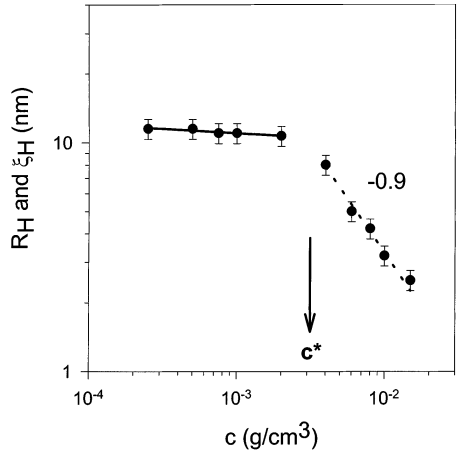

Figure 3. Dependence of the hydrodynamic radius in the dilute regime and of the hydrodynamic correlation length in the semidilute regime on the 85 K hyaluronan concentration in 0.1 M NaCl solutions. The arrow indicates the critical overlap concentration. The black line represents the fit of the data in the dilute regime and the dashed line the fit of the data in the semidilute regime: $\xi_H \approx c^{-0.90}$.

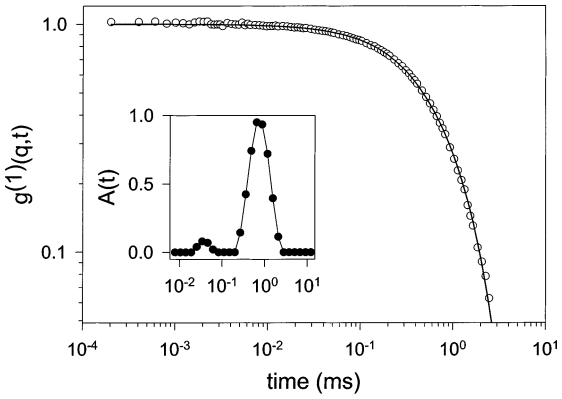

Figure 4. A log−log representation of $g^{(1)}(q,t)$ for $\theta = 100°$ relative to a dilute 6×10^{-3} M NaCl solution at 160 K hyaluronan concentration $c = 1.5 \times 10^{-3}$ g/cm^3 (low ionic strength). The black line represents the fit of $g^{(1)}(q,t)$ using the Contin method, and the inset represents the distribution function of decay times $A(t)$ obtained with the Contin method.

close to that of Gaussian chains (no excluded volume). Also, in the semidilute regime, a slow mode corresponding to polymer associations is measured. This slow mode has already been extensively studied in a previous work;[1,2] therefore, we will not focus our discussion on it.

3.2. Low Ionic Strength Dilute Solutions. In this regime, three ionic strength solutions were investigated: [NaCl] = 6×10^{-3}, 10^{-3}, and 0 M. The hyaluronan molecular weight is equal to 85 K or 160 K depending on the experiment, i.e., depending on the excess salt concentration. For the 10^{-3} M NaCl solution, we used the 85 K hyaluronan sample, whereas for the 6×10^{-3} and 0 M NaCl solutions, we used the 160 K hyaluronan sample.

3.2.1. Dynamic Light Scattering. Figure 4 shows a typical time autocorrelation function of the scattered electric field, $g^{(1)}(q,t)$, obtained for dilute aqueous solutions of hyaluronan at low ionic strength. The inset shows the normalized time distribution function $A(t)$ obtained using the Contin method. The DLS results suggest two well-defined characteristic times for the

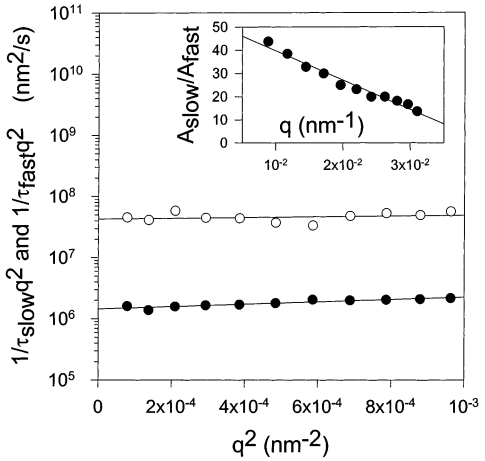

Figure 5. Variation of $1/\tau_{fast}q^2$ (○) and of $1/\tau_{slow}q^2$ (●) with q^2 measured in 6×10^{-3} M NaCl solutions (low ionic strength). The polymer concentration is equal to $c = 1.5 \times 10^{-3}$ g/cm^3. The inset represents the scattering wave vector dependence of A_{slow}/A_{fast}.

relaxation function $g^{(1)}(q,t)$:

$$g^{(1)}(q,t) = A_{fast}(q)\exp\left(\frac{-t}{\tau_{fast}}\right) + A_{slow}(q)\exp\left(\frac{-t}{\tau_{slow}}\right) \quad (23)$$

with $A_{fast}(q) + A_{slow}(q) = 1$. τ_{fast} and τ_{slow} are, respectively, the fast and the slow characteristic relaxation times. $A_{fast}(q)$ and $A_{slow}(q)$ are the corresponding amplitudes. The inspection of Figure 5, representing the variation of $1/\tau_{fast}q^2$ and $1/\tau_{slow}q^2$ with q^2 for a 6×10^{-3} M NaCl 160 K hyaluronan solution at a polymer concentration equal to 1.5×10^{-3} g/cm^3, shows clearly that the fast and slow modes are diffusive with characteristic times, τ_{fast} and τ_{slow}, inversely proportioned to q^2. Thus, it is possible here to calculate the fast and slow diffusion coefficients. Similar results are obtained for [NaCl] = 6×10^{-3}, 10^{-3}, and 0 M aqueous solutions.

Such observed behavior is typical of salt-free semirigid polyelectrolyte solutions. Most of them exhibit slow and fast modes in the spectrum of scattered light. The fast diffusion process of highly charged polyelectrolytes (characterized by a rather large value of the diffusion constant, $D_{fast} = (5.0 \pm 0.6) \times 10^7$ nm^2/s, depending on the ionic strength) has been attributed to coupled diffusion of polyelectrolytes and low molecular weight counterions. In the limit of dilutions large enough to make hydrodynamic interactions negligible,[31,32] one can apply the Nernst−Hartley formula

$$D_{fast} = \frac{(kT/f)D_i(Z+1)}{(kT/f)Z + D_i} \quad (24)$$

where f is the friction factor per unit volume, D_i is the diffusion coefficient of the counterion, and Z is the number of charges carried by the scattering object, the latter being the polymer in dilute regime. Assuming $Z \gg 1$ ($Z > 200$ for our chains), one obtains

$$D_{fast}^{-1} = D_i^{-1} + f/ZkT \quad (25)$$

The friction factor of rigid rods of length $d \approx L_T$ and axial ratio $\rho = d/2b$ (b is the radius of the rod) is given by Broersma's relation[33]

$$f = (3\pi\eta_s d)G(\rho)^{-1} \quad (26)$$

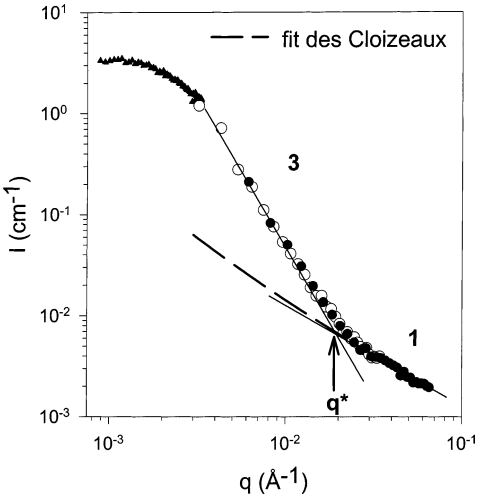

Figure 6. Variation of the scattered intensity with q over three q ranges: $5.95 \times 10^{-4} \leq q$ (Å^{-1}) $\leq 3.31 \times 10^{-3}$ (SLS, ▲); $3.17 \times 10^{-3} \leq q$ (Å^{-1}) $\leq 3.37 \times 10^{-2}$ (○); $6.1 \times 10^{-3} \leq q$ (Å^{-1}) $\leq 6.48 \times 10^{-2}$ (●). The dashed line represents the fit of the data in the q^{-1} part with the des Cloizeaux equation. The NaCl concentration is equal to 6×10^{-3} M (low ionic strength) and the hyaluronan concentration to $c = 1.5 \times 10^{-3}$ g/cm^3. Slopes of 3 and 1 are also represented.

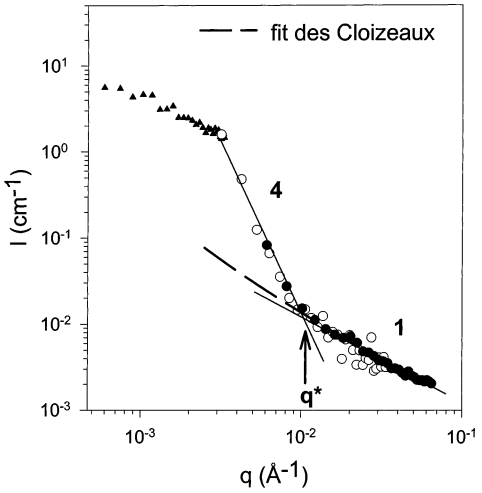

Figure 7. Variation of the scattered intensity with q over three q ranges: $5.95 \times 10^{-4} \leq q$ (Å^{-1}) $\leq 3.31 \times 10^{-3}$ (SLS, ▲); $3.17 \times 10^{-3} \leq q$ (Å^{-1}) $\leq 3.37 \times 10^{-2}$ (○); $6.1 \times 10^{-3} \leq q$ (Å^{-1}) $\leq 6.48 \times 10^{-2}$ (●). Reprinted with permission from ref 17. Copyright 2003 Springer. The dashed line represents the fit of the data in the q^{-1} part with the des Cloizeaux equation. The NaCl concentration is equal to 10^{-3} M (low ionic strength) and the hyaluronan concentration to $c = 1.5 \times 10^{-3}$ g/cm^3. Slopes of 4 and 1 are also represented.

where $G(\rho)$ is given by

$$G(\rho) = \ln 2\rho - \frac{1}{2}\left[1.46 - 7.4\left(\frac{1}{\ln 2\rho} - 0.34\right)^2 - 4.2\left(\frac{1}{2 \ln 2\rho} - 0.39\right)^2\right] \quad (27)$$

Now we focus on the slow mode: there has been some debate about whether the q^{-2}-dependent slow mode of diffusion often reported for dynamic light scattering experiments on low ionic strength polyelectrolyte solutions corresponds to the formation of associations[34,35] or supramolecular structures[31,36−42] or gives evidence of a reptation mechanism.[43] In our case, the increase of A_{slow} with the decrease of q (see the inset in Figure 5) suggests that the slow mode is due to the diffusion of large multichain aggregates. In the present study, we will confirm using SANS experiments (see the next section) the correspondence between the slow polyelectrolyte mode and the formation of associations (see the q^{-4} regime at low q). Moreover, we will clearly show that the association behavior in low ionic strength solutions is similar for flexible and semiflexible polyelectrolytes. In practice, we find $D_{slow} = (1.4 \pm 0.2) \times 10^6$ nm^2/s depending on the excess salt concentration. This gives a hydrodynamic radius $R_H \approx 1750 \pm 250$ Å for the size of the aggregates.

3.2.2. Static Light Scattering and Neutron Scattering. Figures 6−8 show, respectively, the variation of the scattered intensity with q, over the q ranges investigated by SLS and SANS, for NaCl concentration equal to 6×10^{-3}, 10^{-3}, and 0 M. For these low ionic strength solutions, the behavior is profoundly different and unexpected. Indeed, since the electrostatic interactions are not screened, the curve representing the variation of I with q should lead to a "polyelectrolyte peak". This polyelectrolyte peak is not observed. Instead, Figures 6−8 display, when q decreases, a transition from a q^{-1} to a q^{-4} (or q^{-3}; see Figures 6 and 8) dependence (instead of q^{-1} to q^{-2} in the high ionic strength case). The q^{-1} law suggests rodlike particles,

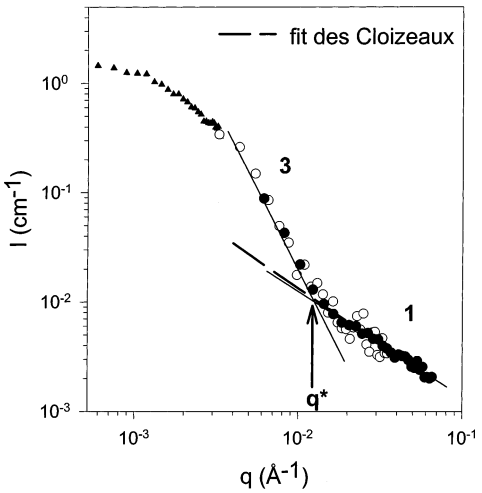

Figure 8. Variation of the scattered intensity with q over three q ranges: $5.95 \times 10^{-4} \leq q$ (Å^{-1}) $\leq 3.31 \times 10^{-3}$ (SLS, ▲); $3.27 \times 10^{-3} \leq q$ (Å^{-1}) $\leq 3.48 \times 10^{-2}$ (○); $6.2 \times 10^{-3} \leq q$ (Å^{-1}) $\leq 6.54 \times 10^{-2}$ (●). The dashed line represents the fit of the data in the q^{-1} part with the des Cloizeaux equation. The NaCl concentration is equal to 0 M (low ionic strength) and the hyaluronan concentration to $c = 1.5 \times 10^{-3}$ g/cm^3. Slopes of 3 and 1 are also represented.

whereas the q^{-4} law suggests compact domains of higher concentration, as often observed in the low-q regime. The existence of large aggregates is confirmed by the light scattering measurements, since the SLS data lead to a large apparent radius of gyration equal to 800 ± 50 Å (M_w = 85 K), to 820 ± 50 Å (M_w = 160 K), and to 1040 ± 50 Å (M_w = 160 K) for [NaCl] = 10^{-3}, 6×10^{-3}, and 0 M, respectively. However, it is difficult to conciliate the SLS curve (smooth descent) with the low-q SANS one (steep descent) in the case of Figure 7. However, since Figure 7 corresponds to a q^{-4} variation at the low q values of the SANS domain, it is known that resolution effects can influence the lowest q values especially for a q^{-4} law. Moreover, the dynamic light scattering experiments described above confirm the

presence of polymer associations, since these measurements display the characteristic well-known q^{-2}-dependent slow polyelectrolyte mode. The value of $R_H \approx 1750$ Å leads to a ratio of $R_H/R_G \leq 2$.

It is surprising that some SANS experiments lead to a q^{-3} dependence and other experiments to a q^{-4} dependence, since the data treatment was the same for all the samples. The first explanation often used for a q^{-3} instead of a q^{-4} dependence is ill-defined surfaces and sizes of the compact scattering objects: undulated surfaces, polydispersity in size. It remains surprising that aggregates would not form the same way depending on the preparation conditions (which are similar), unless their rearrangement is very slow. The second explanation, also classical, is a combination between a q^{-4} law and a q^{-2} law, which would correspond here to the onset of the scattering of the Gaussian chain. A q^{-4} scattering would be better defined if the crossover to a q^{-2} scattering occurs at lower q^*. This seems to be the trend in the data.

We now return to the fact announced above, the absence of the polyelectrolyte peak at low screening. This is certainly due to the strong q^{-4} scattering at low q from aggregates, which probably overlaps the structure factor, in particular if this peak is weak as usually observed in some other natural polymers. In other words, the signal of the aggregates, which are clearly present in these samples, has totally masked the peak in all the experiments carried out at low screening.

What is the origin of this aggregation? To check whether it is due to artifacts in the preparation of the samples, we took a sample investigated at low ionic strength ([NaCl] = 10^{-3} M) and introduced inside one droplet of salted water to drive the salt concentration to 0.1 M, and measured it again. We found again the q^{-2} behavior followed by the q^{-1} behavior as for the sample described in the previous section (3.1). Thus, aggregates seem to be related to the low ionic strength, i.e., to specifically electrostatic interactions. Moreover, these aggregates are stable with time, meaning there is no time dependence for the data. Remember also that SLS measurements were carried out before and after SANS experiments under the same D_2O solutions. No degradation of the purified and filtered hyaluronan solutions was observed. Dynamical measurements done on the same solutions as used for the SANS display the slow polyelectrolyte mode. This confirms the correspondence between the slow polyelectrolyte mode and the formation of associations (q^{-4} regime). To conclude, the behavior observed is very close to that for flexible polyelectrolytes. Association behavior in low ionic strength solutions is similar for flexible and semiflexible charged chains.

3.3. Dependence of the Electrostatic Persistence Length on the Debye Screening Length. The transition between the characteristic q^{-1} rod regime and the q^{-3} (or q^{-4}) regime is marked with q^* in Figures 6−8. Figure 9 shows the SANS data for all the NaCl concentrations on the same figure in the q range where the transition occurs. The value of the transition point q^* can be read to be 0.018 ± 0.002, 0.011 ± 0.001, and 0.012 ± 0.001 Å^{-1} for [NaCl] = 6×10^{-3}, 10^{-3}, and 0 M, respectively. This characteristic crossover q^* in the q dependence of the scattered intensity from a scattering pattern typical for rigid rods to one of aggregates permits a measurement of the total persistence length,

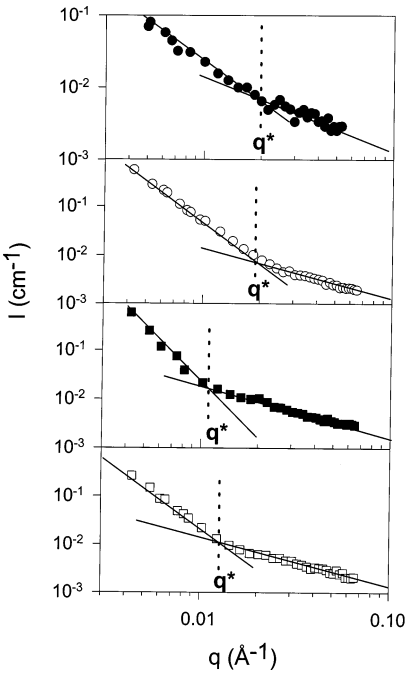

Figure 9. SANS data in the intermediate q range where the transition between the asymptotic q^{-1} regime and the q^{-3} (or q^{-4}) regime (i.e., q^*) occurs for NaCl concentrations equal to 0.1 M (●), 6×10^{-3} M (○), 10^{-3} M (■), and 0 M (□). The hyaluronan concentration is equal to 1.5×10^{-3} g/cm^3.

L_T, of the scattered objects using the following equation:[24]

$$L_T = \frac{1.91}{q^*} \tag{28}$$

We have to keep in mind that eq 28 is derived for a transition from the q^{-1} regime to the q^{-2} regime (when q decreases), as usually visualized in a Kratky plot.[24] This method requires care since the determination of q^* is approximate; however, this gives our best estimate for L_T. Also in this analysis the polydispersity and excluded volume effects have been neglected. However, in the high SANS q range regime, the scattering provides access to the polymer structure on the length scale of L_T and is thus only weakly dependent on interaction and polydispersity effects in this q range.[8] Moreover, the scattering curves at the different ionic strengths are similar in the q^{-1} regime, which indicates and confirms only a weak dependence on interactions and polydispersity in this range of q values. Values of q^* and L_T determined by applying eq 28 as a function of the ionic strength are collected in Table 2. Actually, our procedure has to be taken with great care, since the transition between the q^{-1} regime and the q^{-4} regime is not necessarily related to L_T. The scattering of the polymer associations could overlap the rod to coil transition. In particular, one can imagine that the actual crossover occurs at lower q (giving a larger L_T), this crossover being masked by aggregate scattering.

But we can do more than this simple q^* determination: we can fit the data in the asymptotic regime (corresponding to the q^{-1} rod behavior) with the des Cloizeaux expression (eq 17). We justify that in the q^{-1} regime we can still use the asymptotic expression of des Cloizeaux at low ionic strength. This is because the polydispersity effects are negligible in this regime and this expression is valid in this asymptotic q^{-1} regime

Table 2. Dependence on the Excess Salt Concentration of the Screening Length, the Theoretical Electrostatic Persistence Length (Calculated with the OSF Model), q^*, the Total and Electrostatic Persistence Lengths Determined Using Eq 28, and the Total Persistence Length Determined Using the des Cloizeaux Fit (Eq 17)[a]

[NaCl] (M)	κ^{-1} (Å)	M_w	$L_C = Na$ (Å)	L_e (Å) (OSF eq 2)	q^* (Å^{-1}) (cf. Figure 9)	L_T (Å) (eq 28)	$L_e = L_T - L_0$ (Å) (eq 28)	L_T (Å) (fit with eq 17)	L_c (Å) (fit with eq 17)
0	70.3	160×10^3	4080	84.9	0.012 ± 0.001	159 ± 20	72.5 ± 20	184	3796
10^{-3}	56.8	85×10^3	2170	55.4	0.011 ± 0.001	173 ± 20	86.5 ± 20	135	2200
6×10^{-3}	34.3	160×10^3	4080	20.2	0.018 ± 0.002	106 ± 10	19.5 ± 10	128	3951
0.1	9.5	85×10^3	2170	1.5	0.020 ± 0.002	95.5 ± 10	–	86.5	2311

[a] The molecular weight, the calculated contour length, and the contour length determined with the des Cloizeaux fit are also presented. We used $L_0 = 86.5$ Å.

(which corresponds to almost a decade); i.e., $qL_T > 2$. This allows us to extract the contour length (obtained from the mass per contour length) of the scattered object, equal to $L_c = 2200$ Å for the 10^{-3} M NaCl solution ($M_w = 85$ K) and, respectively, to 3951 and 3796 Å for the 6×10^{-3} and 0 M NaCl solutions ($M_w = 160$ K), i.e., the contour length of a single hyaluronan chain. The 2200 Å value is very close to the value determined at high ionic strength and to the expected theoretical value. This sustains validity for the more interesting fit parameter, L_T. The fits are not very sensitive to the chosen q range, and our best fits are in relatively good agreement with the values obtained using eq 28 (see Table 2). The intrinsic persistence length lies very well within the values expected for this type of polysaccharide, and the fits agree with the mass per unit length of a single hyaluronan chain ($M_L = 40$ (g·mol^{-1})/Å). The parameter $M_L = M/L_c = 39.5 \pm 2$ (g·mol^{-1})/Å (depending on ionic strength) was obtained from the fit of the data only in the asymptotic q^{-1} regime with the des Cloizeaux expression. It is certain that, at larger sizes at low ionic strength, a certain fraction of these chains contributes to aggregate scattering, which is only visible in the q^{-4} law (at larger q this scattering is negligible). The aggregates must be more concentrated than the host solution. The fact that the q^{-1} regime corresponds to the linear mass density of a single hyaluronan chain at the nominal concentration (i.e., global) supports the assumption that most of the chains do not belong to these concentrated aggregates. These facts are observed with several different flexible polyelectrolyte solutions and by several authors.

Theoretical values of the Debye screening length, κ^{-1}, of the electrostatic persistence length, L_e, calculated using Odijk's model (cf. eq 2), and of the contour length, L_c, are compared with the experimental values of L_e and L_c in Table 2 (L_e has been estimated using eq 28, and L_c has been determined from the fit of the data using eq 17). As mentioned before, assuming $L_e = L_T - L_0$, eq 28 gives the best estimate of L_e. For L_0, we used the value obtained at high ionic strength with method 1: $L_0 = 86.5$ Å. The value obtained with method 2, $L_0 = 90$ Å, is also correct and gives the same results for L_e. The variation of the experimental electrostatic persistence length (estimated from eq 28) with the Debye screening length is presented in Figure 10. Also, for [NaCl] = 0.1 M, we used the calculated value $L_e = 1.5$ Å (obtained with OSF eq 2). The results clearly show that these values vary with the salt concentration as predicted by Odijk; i.e., $L_e \approx \kappa^{-2}$ (cf. eq 2). Within the error bars, an $L_e \approx \kappa^{-1}$ law cannot be verified. As mentioned in the Introduction, previous experimental and simulation studies performed under solutions of nonionic wormlike micelles doped with small amounts of ionic surfactants have already checked the OSF theory.[8–10] However, this model was checked for the first time with classical polyelectrolytes.

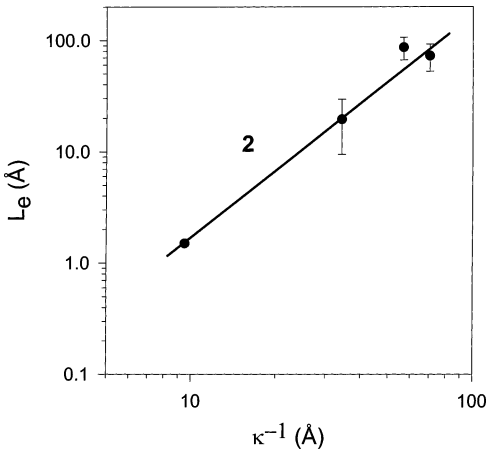

Figure 10. Dependence of the electrostatic persistence length estimated using eq 28 on the Debye screening length κ^{-1}. Reprinted with permission from ref 17. Copyright 2003 Springer. For [NaCl] = 0.1 M, we used $L_e = 1.5$ Å (calculated with OSF eq 2). The black line represents an $L_e \approx \kappa^{-2}$ OSF variation.

Indeed, at low ionic strength, we observe experimentally a marked crossover between the q^{-1} and the q^{-4} (or q^{-3}) regimes, q^* (the rod to coil transition being masked). The apparent persistence length L_T from this crossover position q^* is then a lower bound. On the side of comparison with theory, we observe that this apparent L_T corresponds to the OSF variation, which happens to be the largest predicted, and therefore is a theoretical upper bound. One can summarize as follows: on one hand, we can say that the measured total persistence length appears increased by at least the amount predicted by Odijk for the electrostatic contribution L_e. On the other hand, the OSF variation is the largest predicted.

4. Conclusion

In a combined light and small-Angle neutron scattering study, we have been able to access directly for the first time the conformation of the model semirigid polyelectrolyte polysaccharide hyaluronan. This was possible for high ionic strength dilute solutions, since all repulsions were screened (electrostatic contribution L_e negligible). We thus considered that the scattering was directly proportional to the form factor, and detailed information on the chain flexibility has been obtained from combined SANS and SLS data by applying different fitting procedures based upon expressions for a single-chain scattering function of a wormlike chain without excluded volume. Particular attention has been given to the determination of the intrinsic persistence

length, L_0, and a value close to 90 Å was found using the different fitting methods.

In low ionic strength solutions, the variation of the scattered intensity with q displays a q^{-1} to q^{-4} (or q^{-3} instead of q^{-2}) transition (when q decreases), the latter being characteristic of polymer associations. Moreover, dynamic light scattering measurements display a characteristic slow polyelectrolyte mode, and we show clearly that the association behavior in low ionic strength solutions is similar for flexible and semiflexible polyelectrolytes. This is not likely to be due to hydrophobic defects, but to an organization implying the charges of the counterions and of the chains at low ionic strength. Due to this aggregation, it was difficult to extract the persistence length L_T in this second case. However, since the crossover position is at smaller q than for the screened case, this means that L_T has increased. This increase in L_T, i.e., the contribution from electrostatic interactions, L_e, has been compared with predictions from theoretical models for polyelectrolytes. In particular, the experimental values of L_e as a function of the Debye screening length are in very good agreement with the ones predicted by the OSF model.

List of Key Parameters

$a = 10.2$ Å	length of a monomer unit, which is equal to the distance between two ionic sites
$m = 400$ g/mol	mass of a monomer unit
$\zeta = 0.7$	charge parameter
N	number of monomers in a chain
L_c	weight-average contour length of the chain
L_k	Kuhn length equal to $2L_T$
L_T	total persistence length
L_0	intrinsic persistence length
L_e	electrostatic persistence length
κ^{-1}	Debye−Hückel screening length
c	polymer concentration (g/cm^3)
c_s	excess salt concentration
c_f	free monovalent ion concentration
c^*	overlap concentration
$[\eta]$	intrinsic viscosity of the solution
M_w	weight-average molecular weight
R_G	radius of gyration
A_2	second virial coefficient
R_H	hydrodynamic radius
D	diffusion coefficient
k_D	second dynamical virial coefficient
ξ_H	hydrodynamic correlation length
$I(q)$	absolute scattered intensity (cm^{-1})
$S_2(q)$	interchain scattering factor ("pair term")
$P(q)$	form factor
$S(q)$	solution structure factor

References and Notes

(1) Esquenet, C.; Buhler, E. *Macromolecules* **2002**, *35*, 3708.
(2) Buhler, E.; Rinaudo, M. *Macromolecules* **2000**, *33*, 2098.
(3) Odijk, T. *J. Polym. Sci., Polym. Phys. Ed.* **1977**, *15*, 477.
(4) Skolnick, J.; Fixman, M. *Macromolecules* **1977**, *10*, 944.
(5) Fixman, M. *J. Chem. Phys.* **1982**, *76*, 6346.
(6) Le Bret, M. *J. Chem. Phys.* **1982**, *76*, 6243.
(7) Manning, G. S. *J. Chem. Phys.* **1969**, *51*, 924.
(8) Sommer, C.; Pedersen, J. S.; Egelhaaf, S. U.; Cannavacciuolo, L.; Kohlbrecher, J.; Schurtenberger, P. *Langmuir* **2002**, *18*, 2495.
(9) Cannavacciuolo, L.; Sommer, C.; Pedersen, J. S.; Schurtenberger, P. *Phys. Rev. E* **2000**, *62*, 5409.
(10) Cannavacciuolo, L.; Pedersen, J. S.; Schurtenberger, P. *Langmuir* **2002**, *18*, 2922.
(11) Barrat, J. L.; Joanny, J. F. *J. Phys. II* **1994**, *4*, 1089.
(12) Spiteri, M. N.; Boué, F.; Lapp, A.; Cotton, J. P. *Phys. Rev. Lett.* **1996**, *77*, 5218.
(13) Nishida, K.; Urakawa, H.; Kaji, K.; Gabrys, B.; Higgins, J. S. *Polymer* **1997**, *38*, 6083.
(14) Dubois, E.; Boué, F. *Macromolecules* **2001**, *34*, 3684.
(15) Everaers, R.; Milchev, A.; Yamakov, V. *Eur. Phys. J. E* **2002**, *8*, 3.
(16) Nguyen, T. T.; Shklovskii, B. I. *Phys. Rev. E* **2002**, *66*, 021801.
(17) Buhler, E.; Boué, F. *Eur. Phys. J. E* **2003**, *10*, 89.
(18) de Gennes, P. G. *Scaling Concepts in Polymer Physics*; Cornell University Press: Ithaca, NY, 1979.
(19) (a) Schmitz, K. S. *An Introduction to Dynamic Light Scattering by Macromolecules*; Academic Press: London, 1990. (b) Higgins, J. S.; Benoît, H. C. *Polymers and Neutron Scattering*; Oxford University Press Inc.: New York, 1994.
(20) Koppel, D. E. *J. Chem. Phys.* **1972**, *57*, 4814.
(21) Provencher, S. W. *Makromol. Chem.* **1985**, *82*, 632.
(22) Benoît, H.; Doty, P. *J. Phys. Chem.* **1953**, *57*, 958.
(23) Schmidt, M. *Macromolecules* **1984**, *17*, 553.
(24) (a) Glatter, O.; Kratky, O. *Small Angle X-Ray Scattering*; Academic Press: London, 1982. (b) Denkinger, P.; Burchard, W. *J. Polym. Sci., Part B: Polym. Phys.* **1991**, *29*, 589.
(25) Jerke, G.; Pedersen, J. S.; Egelhaaf, S. U.; Schurtenberger, P. *Langmuir* **1998**, *14*, 6013.
(26) Pedersen, J. S.; Schurtenberger, P. *Macromolecules* **1996**, *29*, 7602.
(27) Sharp, P.; Bloomfield, V. A. *Biopolymers* **1968**, *6*, 1201.
(28) Brûlet, A.; Boué, F.; Cotton, J. P. *J. Phys. II* **1996**, *6*, 885.
(29) des Cloizeaux, J. *Macromolecules* **1973**, *6*, 403.
(30) Burchard, W.; Kajiwara, K. *Proc. R. Soc. London* **1970**, *A316*, 185.
(31) Lin, S. C.; Lee, W.; Schurr, J. M. *Biopolymers* **1978**, *17*, 1041.
(32) Tivant, P.; Turq, P.; Drifford, M.; Magdelenant, H.; Menez, R. *Biopolymers* **1983**, *22*, 643.
(33) Broersma, S. J. *J. Chem. Phys.* **1960**, *32*, 1626.
(34) Ermi, B. D.; Amis, E. J. *Macromolecules* **1998**, *31*, 7378.
(35) Reed, W. F. *Macromolecules* **1994**, *27*, 873.
(36) Mathiez, P.; Mouttet, C.; Weisbuch, G. *Biopolymers* **1981**, *20*, 2381.
(37) Schmitz, K. S.; Lu, M.; Gauntt, J. *J. Chem. Phys.* **1983**, *78*, 5059.
(38) Schmitz, K. S.; Yu, J. *Macromolecules* **1988**, *21*, 484.
(39) Schmidt, M. *Makromol. Chem., Rapid Commun.* **1989**, *10*, 89.
(40) Förster, S.; Schmidt, M.; Antonietti, M. *Polymer* **1990**, *31*, 781.
(41) Sedlák, M.; Amis, E. J. *J. Chem. Phys.* **1992**, *96*, 817.
(42) Ermi, B. D.; Amis, E. J. *Macromolecules* **1996**, *29*, 2703.
(43) Koene, R. S.; Mandel, M. *Macromolecules* **1983**, *16*, 973.

MA0215520